PROPAGATION OF GUIDED WAVES IN DAMAGED FIBER REINFORCED POLYMER LAMINATES: NUMERICAL MODELLING

S. Azadi[1], V. Carvelli[2]

[1] Department A.B.C., Politecnico di Milano, Milan, Italy, shain.azadi@polimi.it
[2] Department A.B.C., Politecnico di Milano, Milan, Italy, valter.carvelli@polimi.it

Keywords: Guided waves, Composite Laminates, Damage, Finite Element Modelling

ABSTRACT

Damage diagnosis in Carbon Fiber Reinforced Polymers (CFRPs) is increasingly crucial due to the rising demand for composite products in several industries. Intralaminar transverse cracks (TCs) are among the most common damages in composite laminates under loading. Hence, early TC detection is vital for reliable structural health monitoring (SHM) and design of CFRP structures. In this study, the TC-induced local wave mode conversion phenomenon is used as a diagnostic tool to identify single TC orientation in a damaged cross-ply CFRP laminate. The TC-induced mode conversion in laminates is modelled using the Finite Element Method (FEM). In the numerical model, Laser-induced Ultrasonic Guided Wave (LUGW) propagation is simulated using an inclined Gaussian laser beam acting on the surface of the laminate. Then, the vertical displacement field of the damaged laminate is analyzed to observe the symmetric (S_0) wave mode conversion into antisymmetric (A_0) mode. Finally, the 2D wavefield is transformed, using 3D-FFT, into the k_x-k_y wavenumber domain and analyzed to verify the presence of A_0 mode components. This method is applied to three orientations of TC to wave direction, namely: 90°, 30°, and 45°, while undamaged plate is considered as reference. The numerical procedure confirmed its capability in early detection and assessment of TC in CFRP laminates.

1 INTRODUCTION

Carbon Fiber Reinforced Polymer (CFRP) laminate is one of the most important structural materials in several engineering fields, such as aerospace and aviation, owing to their high strength-to-weight and stiffness-to-weight ratio, chemical inertness, and durability [1, 2]. Despite the numerous advantages, composite structures are prone to deterioration due to manufacturing defects, extreme operating conditions, impacts, and fatigue [3–5]. Incipient damage modes, ranging from nanometers to micrometers, can compromise CFRPs' structural integrity and operability, ultimately leading to premature failure when undetected.

Intralaminar transverse cracks (TC) are a common damage mechanism in composite laminates involving both matrix and fibers in a ply. These damages can affect global laminate mechanical properties and initiate subsequent damage mechanisms, such as delamination [6, 7]. Hence, improving TC assessment is crucial for designing and monitoring composite structures.

Ultrasonic Guided Waves (UGWs) are a popular non-destructive evaluation (NDE) method, widely adopted for damage diagnosis in composite structures [8–10]. UGWs provide high damage sensitivity, volume coverage, tunable excitation wavelength, and, thanks to the low attenuation, an inspection of inaccessible or internal regions of laminates where traditional techniques may not be feasible [11, 12]. To further increase setup flexibility and minimize physical interferences, such as signal distortions and damages, non-contact ultrasonic techniques were developed to remove the sensor-laminate physical contact requirement. Among non-contact ultrasonic techniques, Laser-induced Ultrasonic Guided Waves (LUGWs) allow remote access to the structure and high-quality data collection from large, complex-shaped, and hard-to-reach components. LUGWs employ an Nd:YAG (neodymium-doped yttrium aluminum garnet) laser to generate a short energy burst focused onto the surface of the laminate, which results in a rapid thermal expansion and contraction of the material that initiates UGW propagation [13, 14]. As for the UGWs' interaction with TCs, several researchers have demonstrated how the presence and density of TCs affect different aspects of UGW propagation in CFRP laminates. High TC density reduces the material stiffness [15], thus increasing its viscoelasticity [16]. When UGW

propagates through the damaged laminate, the wave amplitude decays [17], which can be considered a damage indicator. However, only a high concentration of TCs significantly affects CFRP laminate stiffness, making this approach less effective when detecting TC at its initial stage.

In isotropic materials, the UGW local mode conversion phenomenon at TC has been studied analytically [18] and using Finite Element Analysis (FEA) [19]. This phenomenon is a convenient tool for damage diagnosis, being sensitive to the presence of singular TC, hence useful for the identification of the damage onset. Recent studies showed this phenomenon also in CFRP laminates and used to detect incipient and singular TCs [20].

In this paper, the TC-induced local wave mode conversion phenomenon is predicted using numerical simulations, and results are compared with experimental measurements [20]. The wave mode conversion is then used to establish a damage assessment method sensitive to TC orientation in CFRP laminates. The predicted finite element vertical displacement field visualizes the 2D wavefield highlighting the LUGW propagation in a damaged cross-ply CFRP laminate with a TC in the upper layer. The local wave mode conversion phenomenon, occurring when S_0 interacts with TC, is observed in the k_x-k_y wavenumber domain for different orientations of the TC to the incidence wave.

2 NUMERICAL MODEL FEATURES

2.1 Geometry and material properties

The modeled composite material, illustrated in Fig. 1, is an 8-layer CFRP cross-ply laminate with a stacking sequence of $[90_2/0_2]_S$.

In the finite element model, each ply of the laminate is considered as homogeneous mechanical equivalent elastic material. Hence, according to manufacturer specifications (Toray T7000SC/2500), the components of the anisotropic stiffness matrix of the 0° ply are listed in Table 1.

The laminate plate is 200 mm long and 30 mm wide and has density ρ=1530 kg/m^3. Each ply has a thickness of 0.14 mm, for a total thickness of 1.12 mm. A spatial window, from which the displacement field is recorded, is set from -45 mm to +55 mm (total length 100 mm) along the x-axis, and from -10 mm to +10 mm (total width 20 mm) along the y-axis (see Fig. 1).

The considered damage is an intralaminar transverse crack (TC) positioned in the middle of the plate and covering the entire width. The TC is 0.28 mm deep, affecting the first two plies, and 0.07 mm wide (Fig. 1).

Elastic Stiffness Constants	(GPa)
C_{11}	133.090
C_{12}	4.978
C_{13}	4.978
C_{22}	10.714
C_{23}	5.345
C_{33}	10.714
C_{55}	4.800

Table 1: Mechanical properties of the homogenized CFRP unidirectional ply with 0° fiber orientation (T700SC/2500).

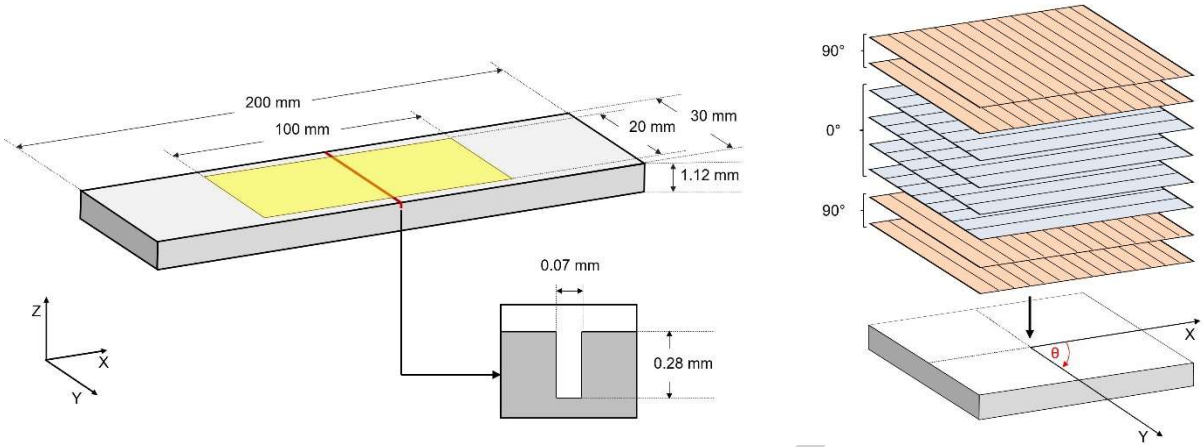

Figure 1: Dimension and stacking sequence of the simulated damaged CFRP laminate with intralaminar transverse crack (TC).

Depending on the mechanical properties, the stacking sequence, the ply thickness, and the wave propagation direction, laminate dispersive properties can be calculated using exact or approximated techniques. In the literature, several methods have been proposed to calculate dispersive properties in complex and anisotropic waveguides, such as Global Matrix Method (GMM), Hybrid Compliance-Stiffness Matrix Method (HCSMM), or Legendre Polynomial Method (LPM) [21–23].

In this research, Semi-Analytical Finite Element (SAFE) method [24, 25] and Fifth-Order Shear Deformation Theory (5-SDT) [26] are used to estimate the dispersion curves, being more efficient and stable [27]. Frequency-wavenumber domains and group velocities for a 0° wave propagation direction are reported in Fig. 2.

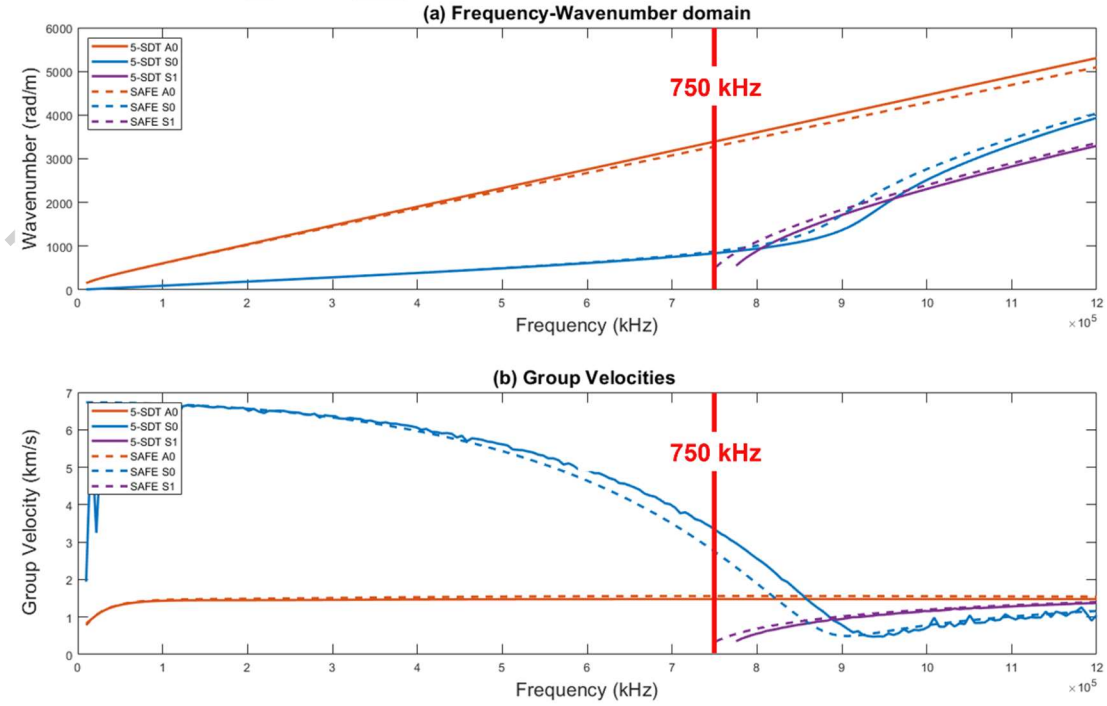

Figure 2: (a) Frequency-Wavenumber domain and (b) Group Velocities of CFRP cross-ply laminate $[90_2/0_2]_s$ calculated using S.A.F.E. method and 5-SDT for a 0° propagating UGW.

To visualize only fundamental wave modes propagating in the material and isolate the mode conversion phenomenon [20], the maximum frequency of interest is selected to be 750 kHz, below which only S_0 and A_0 modes appear.

2.2 Numerical modelling

The multi-physics FEM software COMSOL has been used to simulate thermo-mechanical couplings and wave propagation. Simulating LUGW propagation through dynamic explicit analysis requires accurate spatial and temporal discretization [28].

According to the Nyquist-Shannon theorem, the sampling frequency should be at least twice the goal frequency, set to 750 kHz. For wave propagation problems, spatial discretization follows strict requirements and should be at least half the wavelength of the desired wave mode measured at the goal frequency. According to the dispersion curves in Fig. 2(a), the angular wavenumber of mode S_0 at 750 kHz is about 785 rad/m, or 125 m^{-1}, and the angular wavenumber of mode A_0 at 750 kHz is about 3485 rad/m, or 555 m^{-1}. Therefore, to fully solve wave propagation equations in the laminate, solid hexahedral mesh elements are adopted with maximum dimension d defined according to Eqn. (1).

$$d = \min\left(\frac{1}{k_{S_0} \cdot 10}, \frac{1}{k_{A_0} \cdot 10}\right) \tag{1}$$

Considering wave group velocities $c_g(S_0)$ and $c_g(A_0)$ in Fig. 2(b), plate dimensions are calculated to avoid temporal overlapping between the incoming S_0 and A_0 wave modes, a condition met by adjusting the source-crack distance.

Constraints mimic soft supports by using a spring-like equation having a compressive stiffness equal to the compressive strength of the supports and low tensile stiffness for convergence purposes. A low-reflective boundary condition is used on the outer edges of the plate to isolate wave-crack interaction effects.

The transverse crack is simulated as a prismatic material discontinuity. A dynamic penalty contact, in Eqn. (2), prevents crack faces interpenetration during wave propagation.

$$T_{\mathrm{n}} = \begin{cases} p_{\mathrm{n}} \left\langle \dfrac{\partial g_{\mathrm{n}}}{\partial t} \right\rangle & \text{if } g_{\mathrm{n,old}} \leq 0 \\ 0 & \text{else} \end{cases} \tag{2}$$

In Eqn. (2), p_{n} is the penalty factor, g_{n} is the physical gap distance, and $g_{\mathrm{n,old}}$ is the physical gap at the previous temporal increment. To conserve energy during the initial contact, T_{n} is non-zero during contact only if the physical gap is negative during the increment.

The excitation source for the LUGW propagation is an Nd:YAG laser, which generates a rapid thermal expansion and contraction of the laminate's surface, inducing UGWs in the CFRP plate. According to [14], laser inclination influences the amplitude of the propagating UGW. The numerical model simulates laser illumination through a Gaussian Deposited Beam Power model allowing for a 45°inclination of the beam from the vertical axis. The simulated laser is a Laser Ultrasonic Visualizing Inspector (LUVI) Model CP-1 (Tsukuba Technology Co., Ltd), selected to compare the results with the experimental measurements in [20]. Laser parameters are listed in Table 2.

Parameter	Value	Definition
τ	1e-8 s	Laser pulse duration
a	5e-4 m	Laser beam radius
E_p	1e-4 J	Absorbed pulse energy
I_0	13.2e+9 W/m^2	Laser energy density
P	10.5e+3 W	Laser power output

Table 2: LUVI-CP1 laser properties (Tsukuba Technology Co., Ltd).

Laser energy density is estimated by Eqn.3, where $f(r)$ is the laser spatial variation and $p(t)$ is the laser temporal variation.

$$I_0 = \frac{E_p}{\left(\int_0^\infty f(r) 2\pi r \, dr\right)\left(\int_0^\infty p(t) \, dt\right)} \tag{3}$$

3 RESULTS

3.1 Wave-conversion phenomenon validation

Based on the group velocities in Fig. 2(b) and the laminate geometry, three relevant time instants are selected, i.e., S_0 wave entering the spatial window in Fig. 3(a) and Fig. 4(a), S_0 interacting the TC in Fig. 3(b) and Fig. 4(b), and S_0 exiting the spatial window in Fig. 3(c) and Fig. 4(c).

Fig. 3 represents the normalized (to the maximum) vertical displacement field on the top surface of the plate and plotted in the xy-plane. In Fig. 3(a), only S_0 waves propagate in the spatial window. As suggested by the wavenumber k_x=125m^{-1} at 750 kHz, S_0 waves are distinguishable by the large distances between consecutive peaks. When reaching the TC, waves having smaller peak inter-distances spread in both directions of the damaged region (Fig. 3(b)). This is compatible with the hypothesis of reflected and transmitted A_0 waves because of their higher spatial density (wavenumber of 555 m^{-1}). After 30 µs, the waves propagating from the TC move toward the two sides of the spatial window and interfere with the S_0 waves, as shown in Fig. 3(c).

Further insight into the wave-damage behavior can be obtained by observing the cross-section of the plate in the xz-plane. Fig. 4 presents the normalized vertical displacement field along the entire thickness of the laminate. In Fig. 4(a), the fundamental S_0 mode is detected by its symmetric pattern. Displacement is almost zero along the midplane of the laminate. The upper and lower part has alternating positive and negative displacement of equal amplitude. A different pattern is predicted when the S_0 wave reaches the TC. In Fig. 4(b), the wave reflected and transmitted from the TC has an antisymmetric shape with alternating positive and negative vertical displacements covering the entire thickness. In Fig. 4(c), this pattern is more clearly distinguishable. This initial analysis demonstrates that (i) S_0 waves convert into new waves when interacting with TC, and (ii) these are antisymmetric wave modes. To understand which antisymmetric mode the wave-crack interaction generates, an analysis of the wavenumber domain is necessary. First, the 3D-signal matrix, representing the surface vertical displacement field, is extracted from the numerical model. Then, non-stationary signals are windowed to reduce spectral leakage. A custom Tukey window tapers the non-stationary signal at its endpoints without cutting extended portions of the original signal. The windowed signals are zero-padded up to the closest power of two to increase the computational efficiency of the process, according to the Fast Fourier Transform (FFT) algorithm. Further, this process improves the frequency resolution of the spectrum and reduces spectral leakage. Finally, the post-process 3D-signal matrix is transformed using a 3D-FFT, and the results are plotted in the k_x-k_y wavenumber domain.

Results of numerical simulations and experimental measurements in [20] are compared in Fig. 5 to validate the numerical model. According to the frequency-wavenumber plot in Fig. 2(a), peaks around 555 m^{-1} are associated with the A_0 wave. Therefore, the reflected and transmitted antisymmetric waves from the transverse crack are fundamental A_0 wave modes converted from the S_0 mode. The predicted and experimental wavenumbers are comparable, except for the negative peak associated with the fundamental mode S_0, which has a higher energy content in the opposite direction to the initial wave propagation. This theoretically implies higher energy content in the reflected S_0 wave than the transmitted S_0 one, which agrees with Fig. 4(c), where S_0 waves have a higher amplitude around 30 µs.

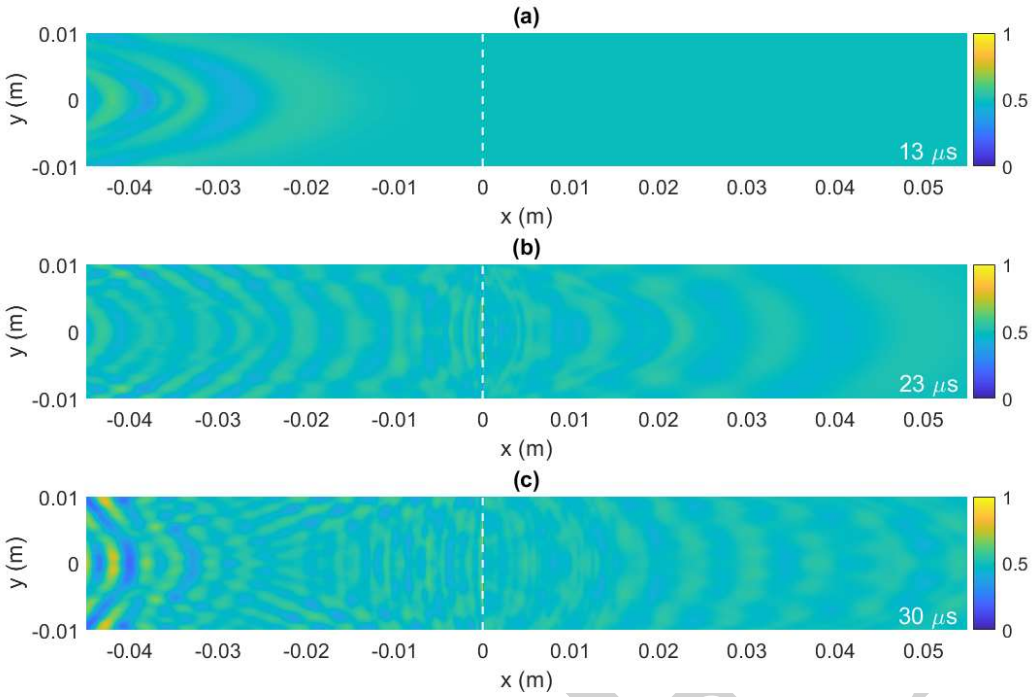

Figure 3: Simulated vertical displacement field measured on the top surface of the CFRP laminate z=1.12 mm (xy-plane) with transverse crack at x=0 mm. Spatial window at time (a) 13, (b) 23, and (c) 30 μs.

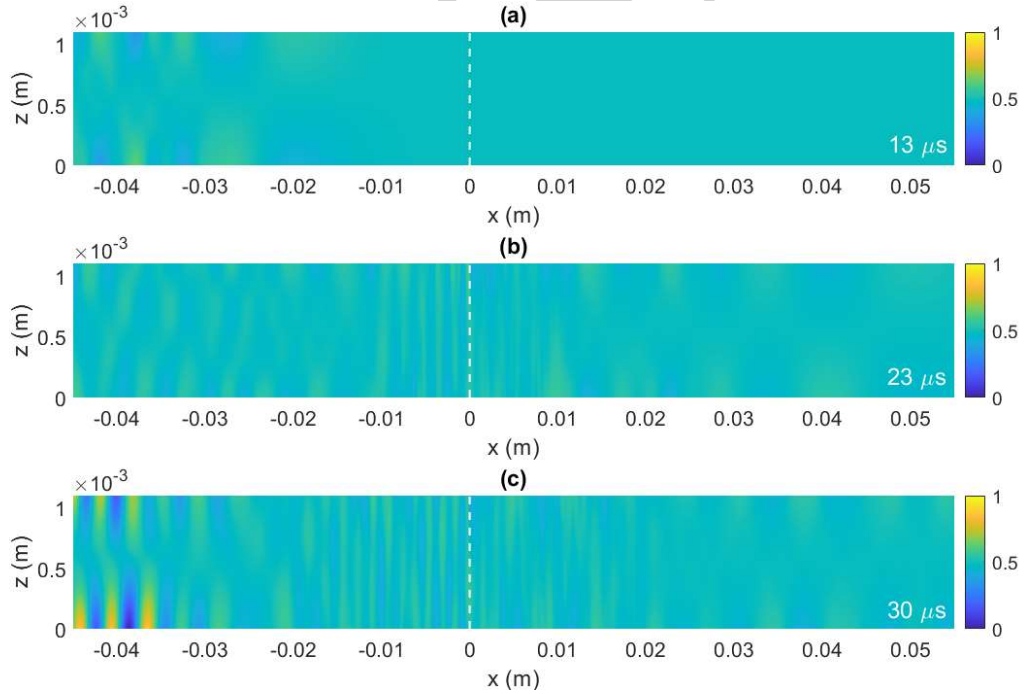

Figure 4: Simulated vertical displacement field measured on the thickness of the CFRP laminate y=0 mm (xz-plane) with transverse crack at x=0 mm. Spatial window at time (a) 13, (b) 23, and (c) 30 μs.

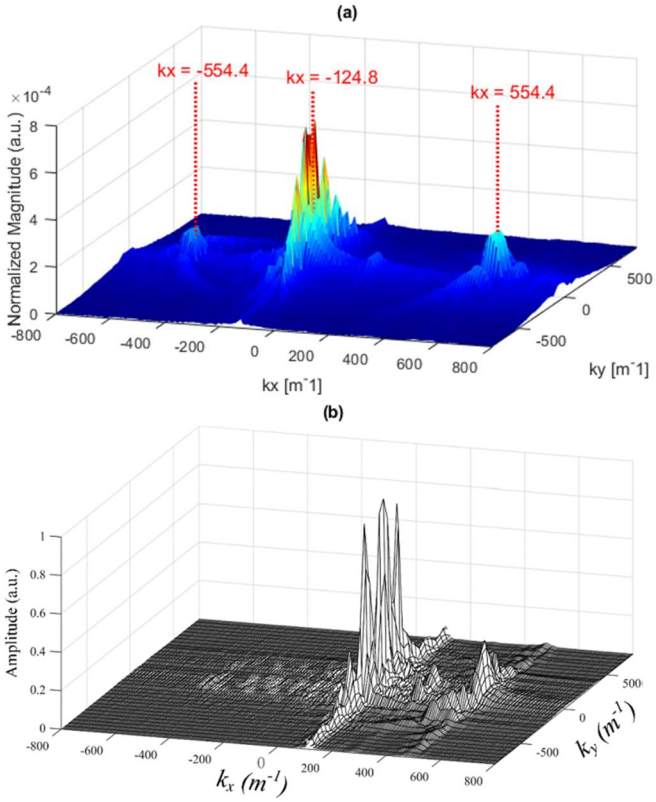

Figure 5: Wavenumber domain comparison: (a) numerical results, (b) experimental measurements [20].

3.2 TC-orientation assessment

The effect of transverse crack orientation on the wavenumber domain is analyzed considering four different scenarios: (i) intact plate, (ii) transverse crack perpendicular to the wave propagation direction (90°), (iii) transverse crack inclined 30° to the wave propagation direction, and (iv) transverse crack inclined 45° to the wave propagation direction.

Results in Fig. 6 show the different crack orientations in the wavenumber k_x-k_y domain. These predictions are comparable in terms of wavenumbers, with the only difference in the negative peak of S_0, which has a higher energy content in the direction opposed to the initial wave propagation, as mentioned above which complies with Fig. 4(c), where S_0 waves have a higher amplitude around 30 μs.

For the undamaged plate, the only wavenumber appearing relates to the S_0 wave mode (Fig. 6(a)), no modal conversion happens without the TC. The TC with different orientations highlights an elliptical-shaped locus of A_0 wavenumbers due to the S_0 modal conversion (Fig. 6(b, c, d)). The peaks related to the A_0 wave mode are located along the line with the same inclination of the TC and passing through the S_0 peak.

Therefore, by observing the wavenumber peaks position of the converted A_0 wave, it is possible to estimate the inclination of the TC damage with respect to the UGW propagation direction.

4 CONCLUSIONS

The proposed numerical approach for the simulation of LUGW propagation in damaged cross-ply CFRP laminates demonstrated its capability in predicting wave-crack interaction.

The proposed approach is based on the local wave-mode conversion, which is a promising method to detect and extract valuable information from the 2D wavefield.

Numerical predictions demonstrated the dependency of magnitude peaks of the converted A_0 wave

mode in the k_x-k_y domain to the angle between TC and wave propagation direction. Thus, this result provides additional information on TC placement and orientation.

To further improve this method, future research will focus on the effect of TC dimension, e.g., length, width, and depth, on the wave conversion phenomenon and its assessment with experimental tests.

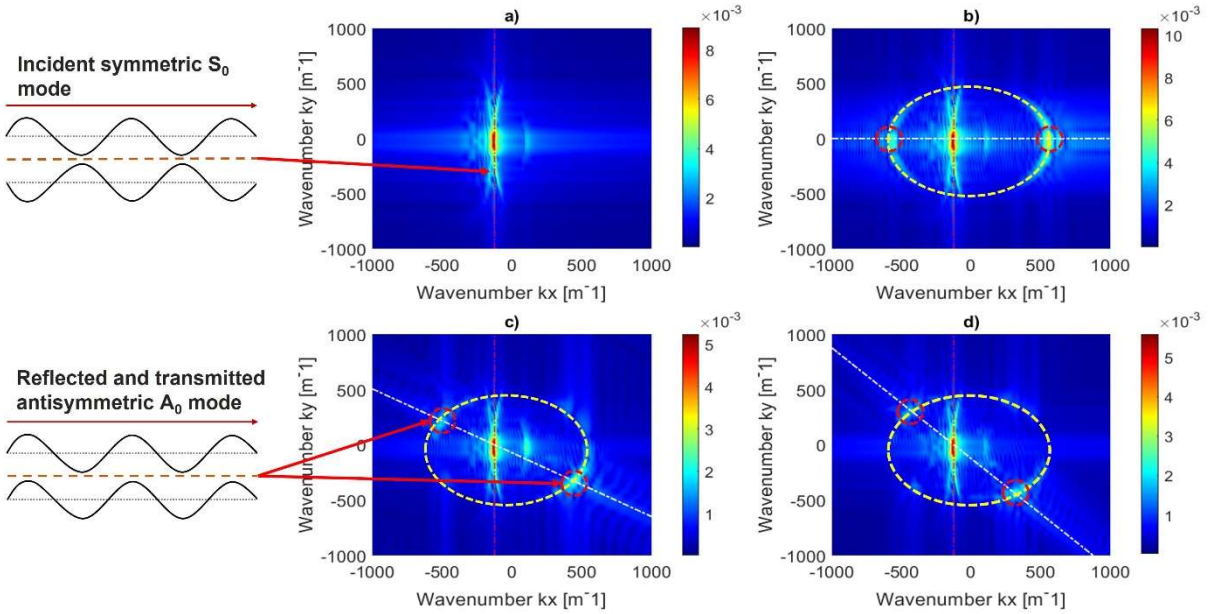

Figure 6: k_x-k_y wavenumber domain for an UGW propagating along the x-axis. (a) intact plate, (b) transverse crack inclined of 90°, (c) transverse crack inclined of 30°, and (d) transverse crack inclined of 45°.

REFERENCES

[1] D. D. L. Chung, Introduction to Carbon Composites, in *Carbon Composites*, Elsevier, 2017, pp. 88–160. (doi: 10.1016/B978-0-12-804459-9.00002-6).

[2] Y. Miyano and M. Nakada, Accelerated testing methodology for durability of CFRP, *Composites Part B: Engineering*, **191**, 2020, p. 107977 (doi: 10.1016/j.compositesb.2020.107977).

[3] R. Talreja, Manufacturing defects in composites and their effects on performance, in *Polymer Composites in the Aerospace Industry*, Elsevier Inc., 2015, pp. 99–113. (doi: 10.1016/B978-0-85709-523-7.00005-0).

[4] S. Abrate, Impact on Laminated Composite Materials, *Applied Mechanics Reviews*, **44**(4), 1991, pp. 155–190 (doi: 10.1115/1.3119500).

[5] P. Alam, D. Mamalis, C. Robert, C. Floreani, and C. M. Ó Brádaigh, The fatigue of carbon fibre reinforced plastics - A review, *Composites Part B: Engineering*, **166**, 2019, pp. 555–579 (doi: 10.1016/j.compositesb.2019.02.016).

[6] N. Takeda and S. Ogihara, Initiation and growth of delamination from the tips of transverse cracks in CFRP cross-ply laminates, *Composites Science and Technology*, **52**(3), 1994, pp. 309–318 (doi: 10.1016/0266-3538(94)90166-X).

[7] S. Ogihara and N. Takeda, Interaction between transverse cracks and delamination during damage progress in CFRP cross-ply laminates, *Composites Science and Technology*, **54**(4), 1995, pp. 395–404 (doi: 10.1016/0266-3538(95)00084-4).

[8] W. Ostachowicz, *Guided waves in structures for SHM : the time-domain spectral element method*, Wiley, 2012.

[9] M. Mitra and S. Gopalakrishnan, Guided wave based structural health monitoring: A review, *Smart Materials and Structures*, **25**(5), 2016, p. 053001 (doi: 10.1088/0964-1726/25/5/053001).

[10] F. Ricci, E. Monaco, N. D. Boffa, L. Maio, and V. Memmolo, Guided waves for structural health monitoring in composites: A review and implementation strategies, *Progress in Aerospace Sciences*, **129**, 2022, p. 100790 (doi: 10.1016/j.paerosci.2021.100790).

[11] G. Zhao, B. Wang, T. Wang, W. Hao, and Y. Luo, Detection and monitoring of delamination in composite laminates using ultrasonic guided wave, *Composite Structures*, **225**, 2019, p. 111161 (doi: 10.1016/j.compstruct.2019.111161).

[12] R. Wang, Q. Wu, K. Xiong, H. Zhang, and Y. Okabe, Evaluation of the matrix crack number in carbon fiber reinforced plastics using linear and nonlinear acousto-ultrasonic detections, *Composite Structures*, **255**, 2021, p. 112962 (doi: 10.1016/j.compstruct.2020.112962).

[13] J. Takatsubo, B. Wang, H. Tsuda, and N. Toyama, Generation Laser Scanning Method for the Visualization of Ultrasounds Propagating on a 3-D Object with an Arbitrary Shape, *Journal of Solid Mechanics and Materials Engineering*, **1**(12), 2007, pp. 1405–1411 (doi: 10.1299/jmmp.1.1405).

[14] O. Saito, N. Higuchi, E. Sen, and Y. Okabe, Analysis of ultrasonic waves generated by oblique incidence of a laser, *Insight - Non-Destructive Testing and Condition Monitoring*, **61**(12), 2019, pp. 714–719 (doi: 10.1784/insi.2019.61.12.714).

[15] N. Toyama, J. Noda, and T. Okabe, Quantitative damage detection in cross-ply laminates using Lamb wave method, *Composites Science and Technology*, **63**(10), 2003, pp. 1473–1479 (doi: 10.1016/S0266-3538(03)00163-5).

[16] A. Mardanshahi, M. M. Shokrieh, and S. Kazemirad, Identification of matrix cracking in cross-ply laminated composites using Lamb wave propagation, *Composite Structures*, **235**, 2020 (doi: 10.1016/j.compstruct.2019.111790).

[17] N. Toyama, T. Okabe, N. Takeda, and T. Kishi, Effect of transverse cracks on lamb wave velocity in CFRP cross-ply laminates, 2002.

[18] C. T. Ng, M. Veidt, L. R. F. Rose, and C. H. Wang, Analytical and finite element prediction of Lamb wave scattering at delaminations in quasi-isotropic composite laminates, *Journal of Sound and Vibration*, **331**(22), 2012, pp. 4870–4883 (doi: 10.1016/j.jsv.2012.06.002).

[19] B. Ren and C. J. Lissenden, Modal content-based damage indicators for disbonds in adhesively bonded composite structures, *Structural Health Monitoring*, **15**(5), 2016, pp. 491–504 (doi: 10.1177/1475921716650627).

[20] F. Yu, O. Saito, and Y. Okabe, Detection of a single transverse crack in a CFRP cross-ply laminate by visualizing mode conversion of Lamb waves, *Composite Structures*, **283**, 2022, p. 115118 (doi: 10.1016/j.compstruct.2021.115118).

[21] L. Knopoff, A matrix method for elastic wave problems, *Bulletin of the Seismological Society of America*, **54**(1), 1964, pp. 431–438 (doi: 10.1785/BSSA0540010431).

[22] E. L. Tan, Hybrid compliance-stiffness matrix method for stable analysis of elastic wave propagation in multilayered anisotropic media, *The Journal of the Acoustical Society of America*, **119**(1), 2006, pp. 45–53 (doi: 10.1121/1.2139617).

[23] J. E. Lefebvre, V. Zhang, J. Gazalet, and T. Gryba, Legendre polynomial approach for modeling free-ultrasonic waves in multilayered plates, *Journal of Applied Physics*, **85**(7), 1999, pp. 3419–3427 (doi: 10.1063/1.369699).

[24] I. Bartoli, A. Marzani, F. Lanza di Scalea, and E. Viola, Modeling wave propagation in damped waveguides of arbitrary cross-section, *Journal of Sound and Vibration*, **295**(3–5), 2006, pp. 685–707 (doi: 10.1016/j.jsv.2006.01.021).

[25] Z. A. B. Ahmad, J. M. Vivar-Perez, and U. Gabbert, Semi-analytical finite element method for modeling of lamb wave propagation, *CEAS Aeronautical Journal*, **4**(1), 2013, pp. 21–33 (doi: 10.1007/s13272-012-0056-6).

[26] A. H. Orta, J. Vandendriessche, M. Kersemans, W. Van Paepegem, N. B. Roozen, and K. Van Den Abeele, Modeling lamb wave propagation in visco-elastic composite plates using a fifth-order plate theory, *Ultrasonics*, **116**, 2021, p. 106482 (doi: 10.1016/j.ultras.2021.106482).

[27] A. H. Orta, M. Kersemans, and K. Van Den Abeele, A comparative study for calculating dispersion curves in viscoelastic multi-layered plates, *Composite Structures*, **294**, 2022, p. 115779 (doi: 10.1016/j.compstruct.2022.115779).

[28] L. Maio and P. Fromme, On ultrasound propagation in composite laminates: advances in numerical simulation, *Progress in Aerospace Sciences*, **129**, 2022, p. 100791 (doi: 10.1016/j.paerosci.2021.100791).